PAPER

Parallel Peak Cancellation Signal-Based PAPR Reduction Method Using Null Space in MIMO Channel for MIMO-OFDM Transmission*

Taku SUZUKI[†], **Mikihito SUZUKI**[†], ***Members***, ***and*** **Kenichi HIGUCHI**[†a)], ***Senior Member***

SUMMARY This paper proposes a parallel peak cancellation (PC) process for the computational complexity-efficient algorithm called PC with a channel-null constraint (PCCNC) in the adaptive peak-to-average power ratio (PAPR) reduction method using the null space in a multiple-input multiple-output (MIMO) channel for MIMO-orthogonal frequency division multiplexing (OFDM) signals. By simultaneously adding multiple PC signals to the time-domain transmission signal vector, the required number of iterations of the iterative algorithm is effectively reduced along with the PAPR. We implement a constraint in which the PC signal is transmitted only to the null space in the MIMO channel by beamforming (BF). By doing so the data streams do not experience interference from the PC signal on the receiver side. Since the fast Fourier transform (FFT) and inverse FFT (IFFT) operations at each iteration are not required unlike the previous algorithm and thanks to the newly introduced parallel processing approach, the enhanced PCCNC algorithm reduces the required total computational complexity and number of iterations compared to the previous algorithms while achieving the same throughput-vs.-PAPR performance.

key words: *OFDM, PAPR, MIMO, beamforming, clipping and filtering, peak cancellation, computational complexity reduction, parallel process*

1. Introduction

The combination of massive multiple-input multiple-output (MIMO) [1], [2], in which a base station transmitter employs a very large number of antennas, using beamforming (BF) and orthogonal frequency division multiplexing (OFDM) signals offers wide-coverage enhanced mobile broadband such as 5G. However, the problem of lowering the peak-to-average power ratio (PAPR) of massive MIMO-OFDM signals must be addressed because of the linearity requirement on the transmitter power amplifier for each of the huge number of antennas. In massive MIMO, the high PAPR of OFDM signals may also be further enhanced due to the variation in the transmission power levels among the transmitter antennas caused by the BF process.

Numerous techniques have been proposed to reduce the PAPR [3]. The clipping and filtering (CF) method [4]–[6] limits the peak envelope of the input signal in the time domain to a predetermined value using a clipping operation. However, the distortion caused by the amplitude clipping is viewed as another source of noise. The CF method can preserve frequency efficiency, but the clipping operation causes in-band interference that cannot be reduced by filtering. References [7] and [8] propose the selected mapping (SLM) method and the partial transmit sequence (PTS) method, respectively. Both the SLM and PTS methods reduce the PAPR by multiplying symbols by each phase factor, which minimizes the PAPR of the input signal in the time domain. These methods require a high level of computational complexity when the number of phase factors is increased. References [9] and [10] investigate PAPR reduction based on the SLM or PTS method considering the artificial bee colony (ABC) algorithm to decrease the high level of computational complexity. The tone reservation (TR) method [11] separates the total number of subcarriers into two parts: the subcarriers for data transmission and those for PAPR reduction signal transmission. The TR method does not interfere with the data symbols but reduces the frequency efficiency.

The PAPR reduction problems in MIMO-OFDM signaling have also been discussed extensively in literature. References [12] and [13] assume the case of no BF. Reference [14] assumes eigenmode MIMO-based BF and applies the SLM and PTS methods. The use of the SLM or PTS method degrades the achievable error rate or throughput of the MIMO-OFDM signal due to a reduced channel coding gain especially in a multiuser MIMO scenario. In downlink massive MIMO, the number of base station transmitter antennas is in general much larger than that of user terminal receiver antennas. Under this assumption, joint optimization of BF, OFDM modulation, and PAPR reduction is investigated in [15]. The tone reservation-based PAPR reduction scheme is investigated in [16]. This kind of approach reduces the frequency efficiency since a part of the transmission bandwidth cannot be used for data transmission. Reference [17] proposes a PAPR reduction method in which some of the transmitter antennas are exclusively used for PAPR reduction in order to remove the in-band interference due to the PAPR reduction signal on the receiver side. However, the method in [17] reduces the BF gain of the data streams since the number of transmitter antennas used for the transmission of data streams is reduced.

Members of our research group reported on an adap-

Manuscript received August 5, 2020.
Manuscript revised October 19, 2020.
Manuscript publicized November 20, 2020.

[†]The authors are with the Graduate School of Science and Technology, Tokyo University of Science, Noda-shi, 278-8510 Japan.

*The material in this paper was presented in part at the 91st IEEE Vehicular Technology Conference (VTC2020-Spring), Antwerp, Belgium, 2020.

a) E-mail: higuchik@rs.tus.ac.jp

DOI: 10.1587/transcom.2020EBT0008

tive PAPR reduction method using the null space in a channel for MIMO-OFDM signals [18]–[20]. This method restricts the peak reduction signal transmitted to only the null space in the given MIMO channel to suppress the degradation in the transmission quality of the data streams that would otherwise be caused by the interference from the in-band peak reduction signal. Since all transmitter antennas are fully utilized for transmitting the data streams, the achievable BF gain of the reported method is higher than that for the method in [17]. It is expected that the effect of the adaptive PAPR reduction method using the null space in the MIMO channel will increase in a massive MIMO scenario, since the dimensions of the null space increase. Members of our research group also investigated the performance of this method in a massive MIMO transmission scenario [21], [22]. We note that [23] investigated the unused beam reservation-based PAPR reduction method, which is similar to the use of null space in a MIMO channel as originally reported in [18]–[20].

In previous investigations by members of our research group [18]–[20], the adaptive PAPR reduction is actualized using an iterative algorithm in which the CF operation and the projection of the peak reduction signal generated by CF onto the null space in the MIMO channel are applied at each iteration. In the following, this method is referred to as the CF followed by the channel-null constraint (CFCNC). Since CFCNC requires the fast Fourier transform (FFT) and inverse FFT (IFFT) operations at each iteration and peak regrowth occurs due to the filtering of out-of-band radiation and the channel null constraint in the peak reduction signal, the required computational complexity is relatively high.

We recently reported a computationally efficient algorithm for the adaptive PAPR reduction method using the null space in a MIMO channel in [24]. The reported algorithm is based on the peak cancellation (PC) signal method originally proposed in [25] and [26] and a channel-null constraint is additionally applied. Hereafter, this algorithm is referred to as the PC with a channel-null constraint (PCCNC). The PC signal is designed so that it has a single dominant peak and satisfies the requirement for out-of-band radiation. By directly adding the PC signal to the time-domain transmission signal at each transmitter antenna, the PAPR is reduced. PCCNC performs PC signal-based PAPR reduction jointly considering all transmission signals for all antennas. Thus, the PC signal is constructed in vector form. By setting the BF vector of the PC signal orthogonal to the MIMO channel, i.e., the BF vector is restricted within the null space in the MIMO channel, the interference to the data streams is eliminated on the receiver side. Since the FFT and IFFT operations are not required at each iteration, the computational complexity of PCCNC is lower than that for conventional CFCNC. However, although PCCNC in [24] significantly reduces the computational complexity, the required number of iterations is rather large, thus a long processing delay may be required since only a single peak in the transmission signals is suppressed at each iteration.

To address the problem, we propose a new PCCNC in which a parallel peak suppression process at each iteration is introduced in order to suppress multiple peaks in the transmission signals at each iteration. By simultaneously adding multiple PC signal vectors to the time-domain transmission signal vector, the number of iterations is effectively reduced. We should consider the fact that when the difference between two target timings of peak signals in a parallel peak suppression process is excessively small, the peak regrowth may be caused by the effect of the superposition of the main and side lobes of multiple PC signals. To address this issue, the newly proposed PCCNC with parallel processing restricts the minimum difference between multiple target timings of peak signals. We show that the newly proposed PCCNC reduces both the required number of iterations and total computational complexity compared to the conventional CFCNC while achieving the same throughput-vs.-PAPR performance. We note that the contents of this paper are based on [27], but include enhanced evaluation and discussions.

The remainder of the paper is organized as follows. First, Sect. 2 briefly describes the principle of the adaptive PAPR reduction method using the null space in the MIMO channel and the conventional CFCNC. Section 3 describes the newly proposed PCCNC. Section 4 presents numerical results based on computer simulations. Finally, Sect. 5 concludes the paper.

2. Adaptive PAPR Reduction Method Using Null Space in MIMO Channel and Conventional CFCNC Algorithm

2.1 Principle of Adaptive PAPR Reduction Method

Here, we briefly explain the principle behind the adaptive PAPR reduction method using the null space in a MIMO channel [18]–[20]. In general, when PAPR reduction is applied to each transmitter antenna independently, the interference component created by the peak reduction signal appears in the transmission frequency band. The adaptive PAPR reduction method using the null space in the MIMO channel limits the transmission of the interference component generated through the PAPR reduction process to just the null space in the MIMO channel. This results in mitigating the throughput reduction due to the interference inherent in PAPR reduction.

The numbers of transmitter and receiver antennas are denoted as N and M, respectively. We assume $N > M$. Therefore, the number of data streams spatially multiplexed is M. In this paper, we assume that the MIMO channel is not frequency-selective for simplicity. The $M \times N$-dimensional channel matrix is denoted as $\mathbf{H}$. The number of subcarriers in the OFDM signal is denoted as K.

Since N is greater than M, we have $N \times (N - M)$-dimensional matrix $\mathbf{V}$ that satisfies $\mathbf{HV} = \mathbf{O}$. We assume that all the $N - M$ column vectors in $\mathbf{V}$ are orthonormalized. Matrix $\mathbf{V}$ corresponds to the null space in MIMO channel $\mathbf{H}$. The frequency-domain N-dimensional effective data trans-

mission signal vector at some subcarrier k after BF is denoted as $\mathbf{x}_{\mathrm{freq},k}$. After the PAPR reduction process is applied at each transmitter antenna, the frequency-domain transmission signal vector at subcarrier k can be represented as

$$\tilde{\mathbf{x}}_{\mathrm{freq},k} = \mathbf{x}_{\mathrm{freq},k} + \boldsymbol{\Delta}_k. \tag{1}$$

Here, $\boldsymbol{\Delta}_k$ is the in-band peak reduction signal vector (interference component to the data stream) added by the PAPR-reduction operation. The adaptive PAPR reduction method using the null space in the MIMO channel limits the transmission of the interference component for PAPR reduction purposes to only the null space in the MIMO channel by BF. More specifically, if $\boldsymbol{\Delta}_k$ can be represented with an $(N-M)$-dimensional vector, $\mathbf{e}_k$, as $\boldsymbol{\Delta}_k = \mathbf{V}\mathbf{e}_k$, the signal vector observed on the receiver side is represented as

$$\mathbf{H}\tilde{\mathbf{x}}_{\mathrm{freq},k} = \mathbf{H}(\mathbf{x}_{\mathrm{freq},k} + \boldsymbol{\Delta}_k) = \mathbf{H}\mathbf{x}_{\mathrm{freq},k} + \mathbf{H}\mathbf{V}\mathbf{e}_k = \mathbf{H}\mathbf{x}_{\mathrm{freq},k}. \tag{2}$$

Since the in-band peak reduction signal is beamformed by $\mathbf{V}$, it does not appear on the receiver side of M antennas as $\mathbf{H}\mathbf{V}\mathbf{e}_k = \mathbf{0}$. Therefore, the PAPR is reduced while the throughput degradation is alleviated.

2.2 Conventional CFCNC

The iterative CFCNC algorithm alternately repeats the PAPR reduction process using the CF operation and restores the restrictions on the peak reduction signal components for actualizing the adaptive PAPR reduction method using the null space in a MIMO channel. Figure 1 shows a block diagram of CFCNC.

In the following, details of the CFCNC process at the j-th iteration ($j = 1, \ldots, J$) are described. The number of iterations is denoted as J. The $\mathbf{e}_k$ vector generated at the j-th iteration is denoted as $\mathbf{e}_k^{(j)}$. At the j-th iteration, the frequency-domain transmission signal vector after BF at subcarrier k, $\mathbf{x}_{\mathrm{freq},k}^{(j)}$, is obtained as

$$\mathbf{x}_{\mathrm{freq},k}^{(j)} = \mathbf{x}_{\mathrm{freq},k} + \mathbf{V}\mathbf{e}_k^{(j-1)}. \tag{3}$$

As the initial setting, $\mathbf{e}_k^{(0)}$ is set to $\mathbf{0}$. Thus, we assume $\mathbf{x}_{\mathrm{freq},k}^{(1)} = \mathbf{x}_{\mathrm{freq},k}$.

At each transmitter antenna, the IFFT is applied to the frequency-domain transmission signal sequence, in which the components of $\mathbf{x}_{\mathrm{freq},k}^{(j)}$ for all subcarriers are collected, and the corresponding time-domain transmission signal sequence is obtained for each transmitter antenna.

Clipping is independently applied to the time-domain transmission signal sequence based on a predetermined threshold. Then, filtering is performed on the clipped signal. In this paper, we assume that filtering to remove the out-of-band radiation caused by the clipping is performed by setting the signal strength of the frequency component corresponding to the out-of-band radiation to zero in the frequency domain by applying the FFT to the clipped time-domain signal. After the above CF process, the frequency-domain transmission signal vector after BF, $\mathbf{x}_{\mathrm{freq},k}^{(j)}$, is assumed to be converted as

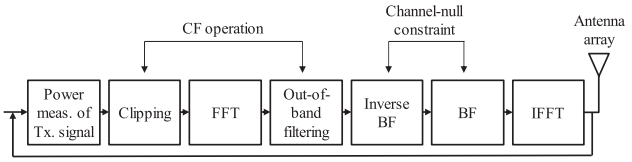

Fig. 1 Block diagram of CFCNC.

$$\tilde{\mathbf{x}}_{\mathrm{freq},k}^{(j)} = \mathbf{x}_{\mathrm{freq},k} + \boldsymbol{\Delta}_k^{(j)}. \tag{4}$$

Here, $\boldsymbol{\Delta}_k^{(j)}$ is the in-band peak reduction signal vector observed at the j-th iteration, which causes interference to the data stream.

To remove the interference component to the data stream, the last step of the process at the j-th iteration restores the restriction that the peak reduction signal is transmitted only to the null space in the MIMO channel. Thus, $\mathbf{e}_k^{(j)}$ is updated as

$$\mathbf{e}_k^{(j)} = \mathbf{V}^H(\tilde{\mathbf{x}}_{\mathrm{freq},k}^{(j)} - \mathbf{x}_{\mathrm{freq},k}) = \mathbf{V}^H\boldsymbol{\Delta}_k^{(j)}. \tag{5}$$

This is the projection of the peak reduction signal to the null space in the MIMO channel.

CFCNC repeats the above process until j reaches J. At the last iteration, $\tilde{\mathbf{x}}_{\mathrm{freq},k}^{(J)}$ is transmitted. CFCNC actualizes the adaptive PAPR reduction method using the null space in a MIMO channel by repeating the CF operation and application of the channel-null constraint on the PAPR reduction signal. However, since the clipping process is performed in the time domain and the filtering process is performed in the frequency domain, the FFT and IFFT operations are required at each iteration as shown in Fig. 1. In addition, peak regrowth occurs due to the filtering of out-of-band radiation and the channel null constraint in the peak reduction signal. Therefore, the computational complexity of CFCNC is relatively high.

3. Proposed PCCNC with Parallel Processing

This section describes the proposed computationally efficient PCCNC algorithm with parallel processing for the adaptive PAPR reduction method using the null space in the MIMO channel. This algorithm is an extension of the per-antenna PC signal-based PAPR reduction method (PAPC) in [25] and [26]. PCCNC performs PC signal-based PAPR reduction jointly considering all transmission signals for all antennas. Thus, the PC signal is constructed in vector form. The PC signal vector is designed so that it is only transmitted to the null space in the MIMO channel and satisfies the out-of-band radiation requirement. By directly adding the PC signal vector to the time-domain transmission signal, the PAPR is reduced while the interference to the data streams

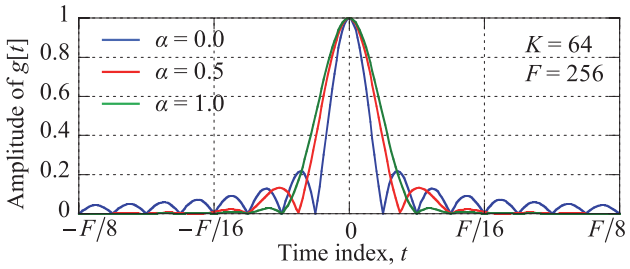

Fig. 2 Basic time-domain signal, $g[t]$.

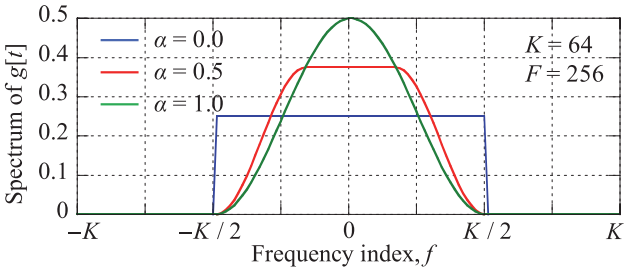

Fig. 3 Spectrum of $g[t]$ in frequency domain.

is eliminated on the receiver side. Since FFT and IFFT operations are not required at each iteration, it is expected that the computational complexity will be reduced compared to that for CFCNC.

The basic time-domain signal, $g[t]$, which is used to generate the PC signal vector, is given as

$$\begin{bmatrix} g[0] \\ \vdots \\ g[F-1] \end{bmatrix} = \mathbf{F}^H \begin{bmatrix} \lambda[0] \\ \vdots \\ \lambda[F-1] \end{bmatrix}, \tag{6}$$

where

$$\lambda[f] = \lambda[F-f] = \begin{cases} \frac{\sqrt{F}}{K}(1+\alpha), & 0 \le f \le \frac{1-\alpha}{1+\alpha} \cdot \frac{K}{2} \\ \frac{(1+\alpha)\sqrt{F}}{2K}\left\{1 - \sin\left(\frac{(1+\alpha)\pi}{\alpha K}\left(f - \frac{K}{2(1+\alpha)}\right)\right)\right\}, & \frac{1-\alpha}{1+\alpha} \cdot \frac{K}{2} < f \le \frac{K}{2} \cdot \\ 0, & \frac{K}{2} < f \le \frac{F}{2} \end{cases} \tag{7}$$

Here, t represents the discrete time index and $t = 0, \ldots, F-1$, where F ($F > K$) is the number of FFT/IFFT points. Matrix $\mathbf{F}$ is the $F \times F$-dimensional FFT matrix whose (m,n)-th element is $e^{-j(2\pi(m-1)(n-1))/F}/\sqrt{F}$. Term $\lambda[f]$ and $\lambda[F-f]$ as a function of frequency index f ($f = 0, \ldots, F/2$) is the spectrum of $g[t]$ that corresponds to the frequency transfer function of the impulse signal. Term $\lambda[f]$ in (7) is defined based on the raised-cosine filter with the roll-off factor of α ($0 \le \alpha \le 1$) in this paper. We note that this paper focuses on baseband signaling, and specifies that the out-of-band radiation requirement is zero for the sake of simplicity. Therefore, the bandwidth of $g[t]$ is fixed to K subcarriers irrespective of α. When $\alpha = 0.0$, $\lambda[f]$ is an ideal rectangular function and $g[t]$ becomes a sinc function. Figures 2 and 3 show $g[t]$ and its spectrum in the frequency domain, respectively, when $K = 64$ and $F = 256$. For any α, $g[t]$ has its maximum peak amplitude of 1.0 at $t = 0$ as shown in Fig. 2 and satisfies the out-of-band radiation requirement of zero for the baseband transmission signal as shown in Fig. 3. As α is set larger, the main lobe of the maximum peak at $t = 0$ becomes wider while the time-domain ripple (side lobe) level decreases more quickly. These properties may affect the peak regrowth issue after PC signal addition and this is quantitatively evaluated in Sect. 4. When $\alpha = 0.0$, the width of the main lobe of the maximum peak at $t = 0$ is $\pm F/K$ discrete times (samples).

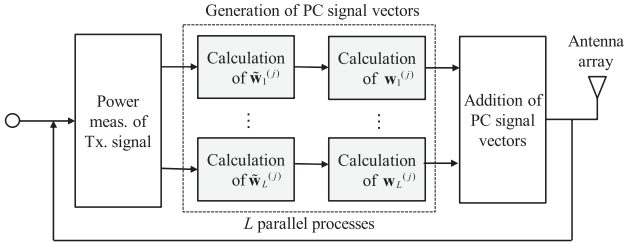

Fig. 4 Block diagram of proposed PCCNC.

Hereafter, the N-dimensional time-domain transmission signal vector before PAPR reduction at time t is denoted as $\mathbf{x}[t]$, whose n-th element is $x_n[t]$.

$$\mathbf{x}[t] = [x_1[t] \quad \cdots \quad x_N[t]]^T. \tag{8}$$

The time-domain transmission signal vector at the j-th iteration of PCCNC is denoted as $\mathbf{x}^{(j)}[t] = [x_1^{(j)}[t] \quad \cdots \quad x_N^{(j)}[t]]^T$. We assume $\mathbf{x}^{(1)}[t] = \mathbf{x}[t]$.

In the following, details of the PCCNC process at the j-th iteration are described. Figure 4 shows a block diagram of PCCNC. The proposed PCCNC tries to suppress in parallel L ($L \le F$) peaks observed at different L time indexes, $\tau_1^{(j)}, \ldots, \tau_L^{(j)}$, at each iteration for a faster processing time. We note that this is different from the initial work on PCCNC in [24].

First, L target time indexes for PAPR reduction at the j-th iteration are determined based on $\mathbf{x}^{(j)}[t]$. This is basically done by finding L timings where the L-highest peaks are observed. However, as is presented hereafter, when the difference between two target time indexes is excessively small, the negative impact of the superposition of the main lobe of the PC signals (shown in Fig. 2) on the peak regrowth after the addition of multiple PC signals must be addressed. To address this issue, we apply a restriction to the minimum time difference, δ, between the L selected target time indexes. Parameter δ ($\delta > 0$) controls the minimum difference between $\tau_l^{(j)}, \ldots, \tau_L^{(j)}$.

The selection of $\tau_1^{(j)}, \ldots, \tau_L^{(j)}$ is performed as follows. First, the time index, where $x_n^{(j)}[t]$ has the maximum amplitude for all n and t, is selected as $\tau_1^{(j)}$. After that, $\tau_l^{(j)}$ ($l = 2, \ldots, L$) is determined in sequential manner as

$$\tau_l^{(j)} = \arg\max_t \left(\max_n |x_n^{(j)}[t]|\right) \quad \text{for } t \in \{0, \ldots, F-1\} \backslash \bigcup_{l'=1,\ldots,l-1} \{\tau_{l'}^{(j)} - \delta, \ldots, \tau_{l'}^{(j)} + \delta\}. \tag{9}$$

Then, all the l-th ($l = 1, \ldots, L$) PC signal vectors, $\mathbf{p}_l^{(j)}[t]$, which are represented in the form of (10), are added to $\mathbf{x}^{(j)}[t]$ to reduce simultaneously the peak power observed at the L different timing indexes.

$$\mathbf{p}_l^{(j)}[t] = -\mathbf{w}_l^{(j)} g\left[t - \tau_l^{(j)}\right]. \tag{10}$$

$$\mathbf{x}^{(j+1)}[t] = \mathbf{x}^{(j)}[t] + \sum_{l=1}^{L} \mathbf{p}_l^{(j)}[t]. \tag{11}$$

Basic signal $g[t]$ has its maximum peak amplitude of 1.0 at $t = 0$. The l-th PC signal vector, $\mathbf{p}_l^{(j)}[t]$, is generated from the $\tau_l^{(j)}$-time-shifted version of $g[t]$, $-g[t - \tau_l^{(j)}]$, by applying BF with the BF vector of $\mathbf{w}_l^{(j)}$. By adding $\mathbf{p}_l^{(j)}[t]$ to $\mathbf{x}^{(j)}[t]$, the peak power observed at $t = \tau_l^{(j)}$ is suppressed by the peak signal portion of $g[0]$, while the impact of adding the PC signal to the other timing is mitigated.

An important component of the PC signal vector, $\mathbf{p}_l^{(j)}[t]$ is its BF vector $\mathbf{w}_l^{(j)}$. The N-dimensional vector $\mathbf{w}_l^{(j)}$ should lie within the null space in the MIMO channel. PC signal vector $\mathbf{p}_l^{(j)}[t]$ beamformed by $\mathbf{w}_l^{(j)}$ satisfies the requirements for the zero interference to the data streams. This is because the PC signal is transmitted to only the null space in the given MIMO channel and does not appear on the receiver side. In this paper, $\mathbf{w}_l^{(j)}$ is calculated as

$$\tilde{\mathbf{w}}_l^{(j)} = \begin{bmatrix} \tilde{w}_{l,1}^{(j)} & \cdots & \tilde{w}_{l,N}^{(j)} \end{bmatrix}^T$$

$$\tilde{w}_{l,n}^{(j)} = \begin{cases} x_n^{(j)}[\tau_l^{(j)}] - A_{\text{th}} e^{j\theta_n^{(j)}[\tau_l^{(j)}]}, & |x_n^{(j)}[\tau_l^{(j)}]| > A_{\text{th}} \\ 0, & \text{Otherwise} \end{cases} \tag{12}$$

$$\mathbf{w}_l^{(j)} = \mathbf{V}\mathbf{V}^H \tilde{\mathbf{w}}_l^{(j)}. \tag{13}$$

Here, $\theta_n^{(j)}[\tau_l^{(j)}]$ is the phase of $x_n^{(j)}[\tau_l^{(j)}]$. Term A_{th} is the predetermined amplitude threshold for PAPR reduction. Vector $\tilde{\mathbf{w}}_l^{(j)}$ is an ideal peak reduction vector in the sense that if vector $\tilde{\mathbf{w}}_l^{(j)}$ calculated in (12) is used as $\mathbf{w}_l^{(j)}$ in (10), the amplitude levels of the transmission signals for all N antennas at time $\tau_l^{(j)}$ (thus, $\left|x_n^{(j)}[\tau_l^{(j)}]\right|$ for all n) can simultaneously be set equal to or lower than A_{th}. However, vector $\tilde{\mathbf{w}}_l^{(j)}$ has a component that is orthogonal to the null space in the MIMO channel (thus, $\mathbf{H}\tilde{\mathbf{w}}_l^{(j)} \neq 0$), which causes interference to the data streams. Therefore, $\tilde{\mathbf{w}}_l^{(j)}$ is projected onto the null space in MIMO channel $\mathbf{V}$ to generate $\mathbf{w}_l^{(j)}$ using (13).

PCCNC repeats the above process until j reaches J. Since the FFT and IFFT operations are not needed at each iteration as shown in Fig. 4, PCCNC is expected to achieve a lower level of computational complexity and number of iterations than that for the conventional CFCNC. In addition, PCCNC with parallel processing reduces the number of iterations (in other words, the processing delay time) compared to that for PCCNC without parallel processing.

4. Numerical Results

4.1 Simulation Parameters

The number of transmission antennas, N, is set to 64 or 128. The number of receiver antennas, M, is fixed at 4. The number of subcarriers, K, is 64. We mainly use the number of FFT/IFFT points, F, of 256, which corresponds to the F/K of 4-times oversampling in the time domain in order to measure a satisfactorily accurate PAPR level [28]. However, to evaluate in detail the relationship between an appropriate δ and L by further increasing the time resolution, we assume the F of 1024 (16-times oversampling) only in Fig. 7. For evaluation generality, we assume that the signal constellation of each subcarrier follows an independent standard complex Gaussian distribution. Assuming multiuser MIMO, zero-forcing BF is applied. As the channel model, we assume flat Rayleigh fading, which is independent between transmitter antenna branches and between receiver antenna branches. The signal-to-noise ratio (SNR) is set to 10 dB.

As the adaptive PAPR reduction method using the null space in the MIMO channel, conventional CFCNC and the proposed PCCNC are tested. As a per-antenna independent PAPR reduction method, the per-antenna CF (PACF) and PAPC are also tested for comparison. PAPC is assumed to employ L-parallel processing per iteration as in PCCNC. For all methods, the number of iterations, J, is parameterized. In PAPC and PCCNC, L, δ, and α are also parameterized. In PCCNC, after J iterations, PAPC is assumed to be performed with $J_{\text{add}} = J/10$ iterations in order to achieve a lower PAPR at the cost of reduced throughput for the purpose of clear comparison to CFCNC.

The power threshold, $P_{\text{th}} = |A_{\text{th}}|^2$, in the PAPR reduction process is defined as the signal power threshold normalized by the signal power per antenna averaged over the channel realizations. The PAPR is defined as the ratio of the peak signal power to the average signal power across all the transmitter antennas per OFDM symbol. The sum throughput of M streams (users) is calculated based on the Shannon formula taking into account the Bussgang theorem [29].

4.2 Simulation Results

First, we evaluate the effect of the restriction on the minimum time difference, δ, for the proposed PCCNC with parallel processing. Figure 5 shows the average PAPR as a function of δ for PCCNC with N as a parameter. Parameters J and L are set to 10 and 32, respectively. The roll-off factor, α, of the PC signal is set to 0.0. Threshold P_{th} is set to 3 dB and 7 dB. Both the N of 64 and 128 are evaluated. When P_{th} is 7 dB, the average PAPR is almost constant regardless of δ. However, when P_{th} is 3 dB, the average PAPR of PCCNC with δ of 1 is very high. This observation does not depend on N. This is due to the peak regrowth caused by the superposition of the main lobe of the PC signal among L-parallel

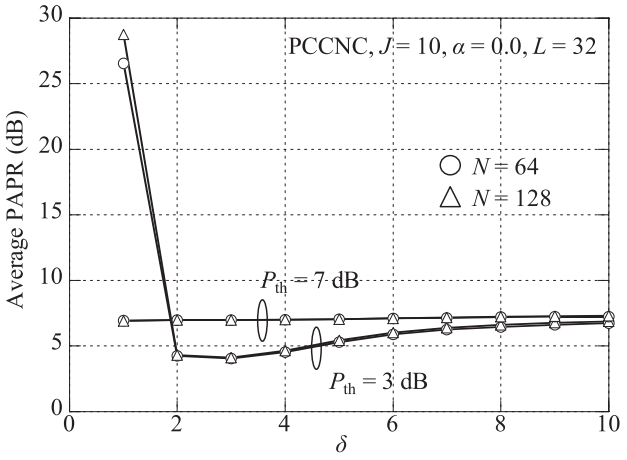

Fig. 5 Average PAPR as a function of δ with N as a parameter.

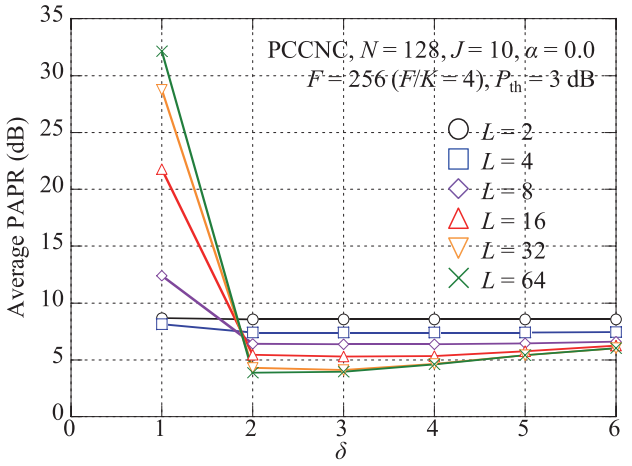

Fig. 6 Average PAPR as a function of δ with L as a parameter ($F/K = 4$).

processes. Furthermore, the average PAPR increases when using an excessively large δ. This is because in this case the degrees of freedom in selecting L target peaks are limited.

Figures 6 and 7 show the average PAPR as a function of δ for PCCNC with L as a parameter. Figure 6 assumes the F of 256 that corresponds to the oversampling factor F/K of 4 and is the same as in the other evaluations. In Fig. 7, F is set to 1024 so that the oversampling factor is increased to 16 and the time resolution is 4-times finer than that in Fig. 6 in order to measure precisely the impact of L on the best δ value. Terms N, J, and α are set to 128, 10, and 0.0, respectively. Threshold P_{th} is set to 3 dB. Figures 6 and 7 show that the use of an excessively small δ results in degradation in the achievable PAPR. This is because the probability of the peak regrowth caused by the L-parallel process increases due to the superposition of the main lobe of multiple PC signals added in parallel to the transmission signal at each iteration. This degradation is significant when L is large. When using an excessively large δ, the PAPR increase is also observed especially when L is large. This is because in this case the degrees of freedom in selecting L target peaks is limited and PCCNC must perform PC-signal addition to the limited number of peak signals, which is less than L, at each iteration. Figure 7 shows that as L is increased the impact of the δ selection on the achievable PAPR becomes clearer and the best δ value decreases. This is due to the tradeoff between the negative impact of the superposition of the main lobe of multiple PC signals and the degrees of freedom in selecting L target peaks. With an appropriate choice for δ, the achievable PAPR is reduced as L is increased thanks to the parallel processing at each iteration.

However, the variations in the best δ values for different L settings are not significant. When we assume a practical oversampling factor, F/K, of 4 using F of 256 as in Fig. 6, the best δ is approximately 3 irrespective of the L value. This corresponds to 75% of the main lobe width of the main peak for a PC signal with α of 0.0, i.e., $\pm F/K = 4$.

Next, we evaluate the impact of the roll-off factor, α, of the PC signal on the average PAPR as a function of δ.

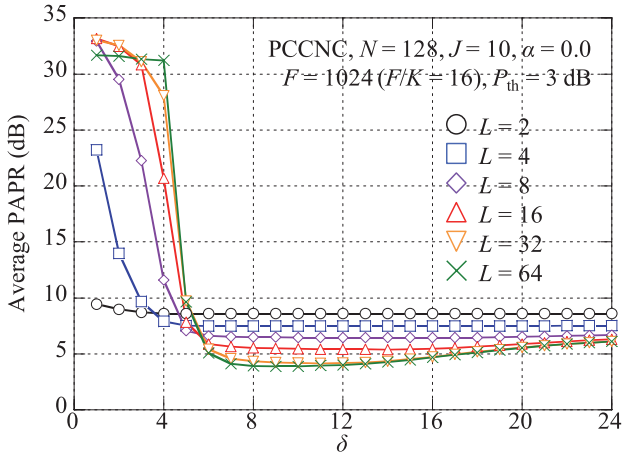

Fig. 7 Average PAPR as a function of δ with L as a parameter ($F/K = 16$).

Figure 8 shows the average PAPR as a function of δ with α as a parameter. Terms N, J, L, and P_{th} are set to 128, 10, 32, and 3 dB, respectively. The overall performance tendency is the same for all tested α values. As α is increased, the PAPR degradation at $\delta = 2$ is slightly increased. The reason for this can be understood in Fig. 9. Figure 9 shows the maximum interference power levels of a PC signal observed outside the restricted δ-time durations, which is normalized by the peak power of $g[0]$. This interference level is a source of peak regrowth. The main lobe of the PC signal becomes wider as α is increased as shown in Fig. 2. The PC-signal interference becomes higher when α is large for a relatively small δ regime, although the ripple (side lobe) level decreases more quickly, which corresponds to a lower interference level for large δ values. In conclusion, the best δ is approximately constant for various α settings assuming a practical oversampling factor, and $\alpha = 0.0$ achieves the best PAPR performance.

Figure 10 shows the average PAPR as a function of J for PCCNC with δ as a parameter. Terms N, α, L, and P_{th} are set to 128, 0.0, 32, and 3 dB, respectively. The δ values

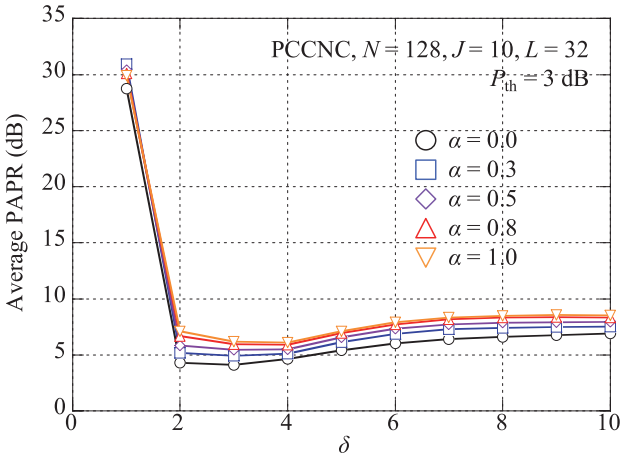

Fig. 8 Average PAPR as a function of δ with α as a parameter.

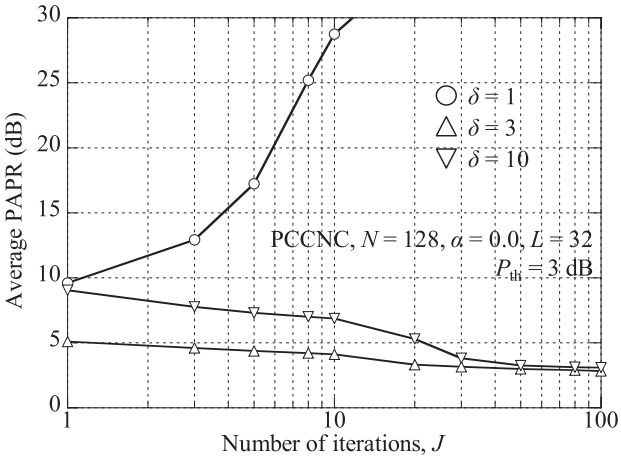

Fig. 10 Average PAPR as a function of number of iterations, J.

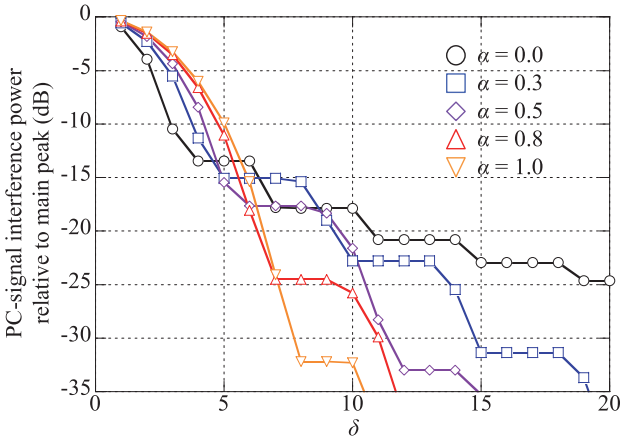

Fig. 9 PC-signal interference power relative to main peak as a function of δ with α as a parameter.

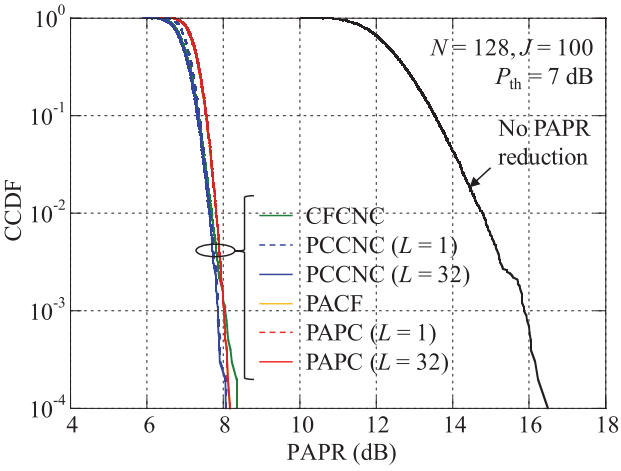

Fig. 11 CCDF of PAPR.

of 1, 3, and 10 are tested. When J is increased, the average PAPR of PCCNC with $\delta = 1$ is significantly increased. Meanwhile, as δ is increased to 3 or 10, the reduction in the average PAPR is enhanced. This confirms that the restriction on the minimum time difference, δ, helps PCCNC with parallel processing work well. When comparing PCCNC using $\delta = 3$ to that using $\delta = 10$, PCCNC using $\delta = 3$ reduces the required number of iterations for achieving the same average PAPR than that for $\delta = 10$. This is because by setting the best δ value, PCCNC with parallel processing achieves peak reduction more efficiently at each iteration. Figures 5–10 show that the δ of 3 with $\alpha = 0.0$ is the best for the proposed PCCNC with parallel processing from the viewpoint of the achievable PAPR performance under the assumed simulation conditions. In the following evaluation, α and δ are set to 0.0 and 3, respectively, for PAPC and PCCNC.

From here, we compare the proposed PCCNC with conventional CFCNC and the per-antenna independent PAPR reduction approach such as PACF and PAPC. Figures 11 and 12 show the complementary cumulative distribution function (CCDF) of the PAPR and throughput, respectively. N is set to 128. P_{th} and J are set to 7 dB and 100, respectively. The L of 1 and 32 are evaluated. The PAPR distributions of all PAPR reduction methods are quite comparable regardless of L. The throughput levels for CFCNC and PCCNC (shown in overlapped green and blue lines) are very close to that without PAPR reduction and much better than those for PACF and PAPC (shown in overlapped orange and red lines), irrespective of L. This is because the peak reduction signal is concentrated in the null space in the MIMO channel in CFCNC and PCCNC; therefore, it does not interfere with the data stream on the receiver side. This confirms that PCCNC with parallel processing works well.

Figure 13 shows the average throughput as a function of the average PAPR for PCCNC and PAPC with L as a parameter. The relationship between the average PAPR and average throughput is varied by changing the P_{th} value for the PCCNC and PAPC methods. N and J are set to 128 and 100, respectively. For PCCNC, the achievable throughput-vs.-PAPR performance for $L = 1$ is degraded compared to that for $L = 32$ or 64. This is because $J = 100$ and $J_{\text{add}} = 10$ in PCCNC are insufficient to suppress all peaks in

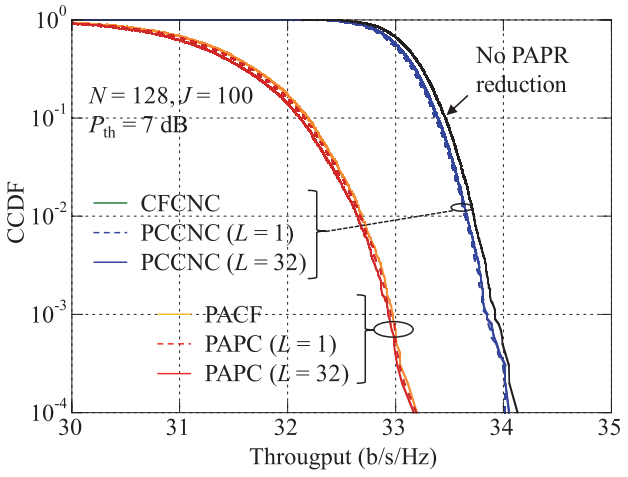

Fig. 12 CCDF of throughput.

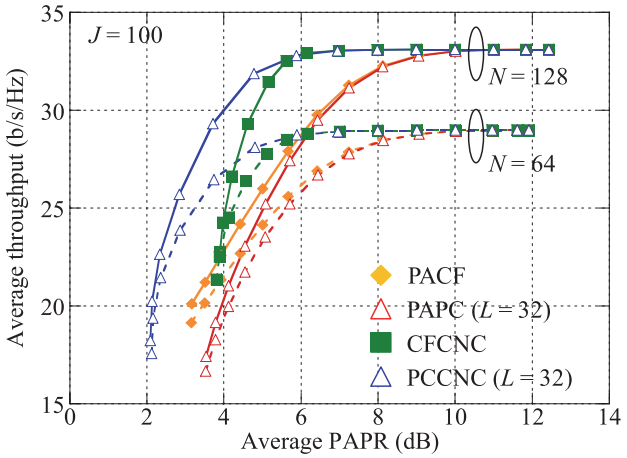

Fig. 14 Average throughput as a function of average PAPR for respective PAPR reduction methods with N as a parameter.

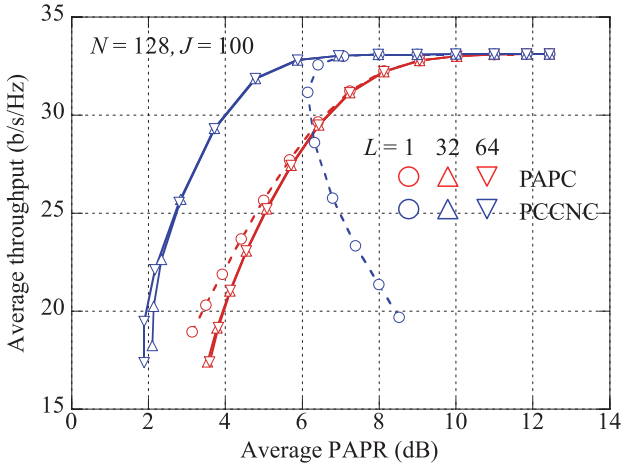

Fig. 13 Average throughput as a function of average PAPR for PCCNC and PAPC with L as a parameter.

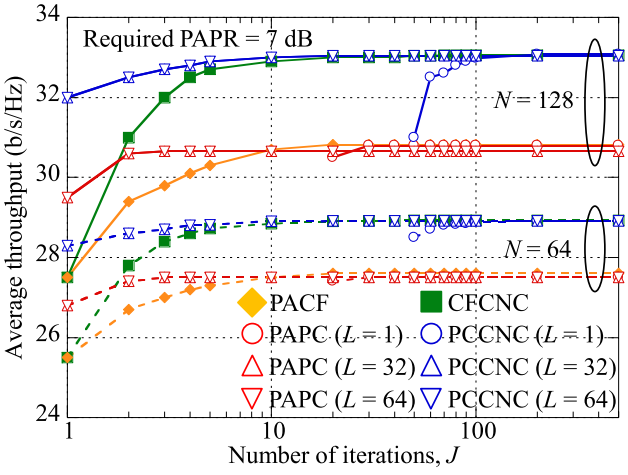

Fig. 15 Average throughput as a function of number of iterations, J.

the transmission signal when L is 1 since only a single peak is suppressed per iteration. Regardless of L, PAPC achieves comparable throughput-vs.-PAPR performance in the high PAPR region. Meanwhile, the achievable performance of PAPC is degraded in the low PAPR region when L is increased to 32 or 64. This is because L PC signals are added independently to each transmitter antenna per iteration and the in-band interference from the PC signals is increased as L becomes large. This degradation is not observed in PCCNC since the interference to the data streams is eliminated on the receiver side.

Figure 14 shows the average throughput as a function of the average PAPR for the respective PAPR reduction methods with N as a parameter. The relationship between the average PAPR and average throughput is varied by changing the P_{th} value for the respective PAPR reduction methods. J and L are set to 100 and 32, respectively. When using the per-antenna PAPR reduction approaches such as PACF and PAPC, the degradation in the throughput accompanying the reduction in the PAPR is large. This degradation is remarkable especially when N is large. This is because the interference from the peak reduction signal becomes a dominant factor in the degradation in the throughput when N is large as the increased BF gain diminishes the impact of receiver noise. On the other hand, the adaptive PAPR reduction method using the null space in the MIMO channel employing CFCNC and PCCNC mitigates the degradation in the throughput caused by the reduction in the PAPR. Focusing on PCCNC and CFCNC, PCCNC achieves better throughput-vs.-PAPR performance than CFCNC. This is due to circumventing the peak regrowth caused by the filtering of out-of-band radiation in CF-based approach.

Figure 15 shows the average throughput as a function of J for a given PAPR requirement. The required average PAPR is set to 7 dB. Both the N of 64 and 128 are evaluated. L is parameterized from 1, 32, to 64. Regardless of N, the required number of iterations of PCCNC with $L = 1$ for achieving the same throughput is much larger than that for CFCNC. However, as L is increased to 32 or 64, PCCNC reduces the required number of iterations compared to that for CFCNC. This is because L peak signals can be sup-

Table 1 Number of real multiplications per iteration for respective PAPR reduction methods.

PAPR reduction method		Process	Number of real multiplications
Per-antenna PAPR reduction method	PACF	Power meas. of transmission signal	$2NF$
		Amplitude clipping	$3NF$
		FFT	$4NF\log_2 F$
		IFFT	$4NF\log_2 F$
	PAPC	Power meas. of transmission signal	$2NF$
		Time shift of $g[t]$	0
		Calculation of amplitude and phase	$2NL$
		Generation of PC signal	$LN(2+F)$
Adaptive PAPR reduction method using null space in MIMO channel	CFCNC	Power meas. of transmission signal	$2NF$
		Amplitude clipping	$3NF$
		FFT	$4NF\log_2 F$
		Inverse BF (projection on to null space)	$4FN(N-M)$
		BF	$4FN(N-M)$
		IFFT	$4NF\log_2 F$
	PCCNC	Power meas. of transmission signal	$2NF$
		Time shift of $g[t]$	0
		Calculation of amplitude and phase	$4LN(N+1)$
		Generation of directional vector $\mathbf{w}^{(l)}$	
		Generation of PC signal vector	LNF

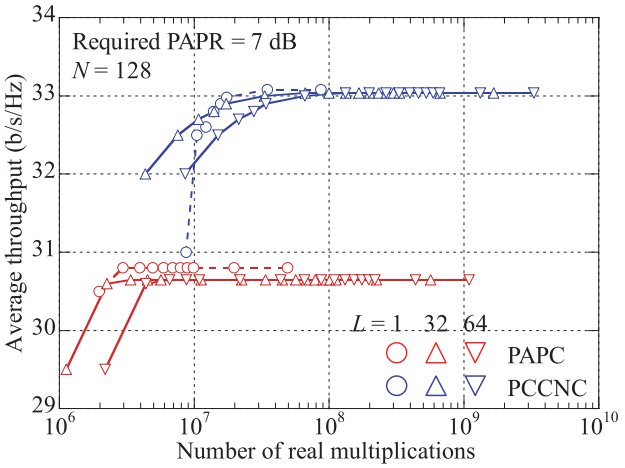

Fig. 16 Average throughput as a function of number of real multiplications of PCCNC and PAPC with L as a parameter.

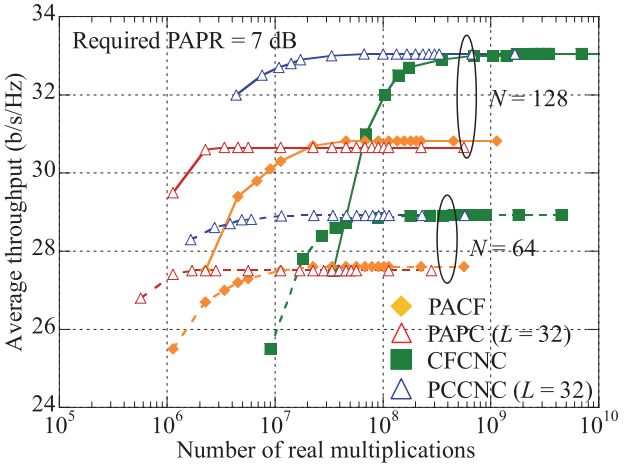

Fig. 17 Average throughput as a function of number of real multiplications for respective PAPR reduction methods.

pressed in parallel by multiple PC signals at each iteration. Therefore, PCCNC with parallel processing reduces the required number of iterations and mitigates the delay time of the PAPR reduction process compared to CFCNC and PCCNC without parallel processing while achieving comparable throughput-vs.-PAPR performance levels. We note that PAPC with L-parallel processing achieves a better tradeoff than PACF as well.

Since the required calculation cost per iteration is different among all the evaluated methods, in the following we compare the throughput-vs.-PAPR performance levels of all methods for the same computational complexity. In this paper, we use the required number of real multiplications for each method to evaluate the computational complexity. Table 1 gives the number of real multiplications per iteration required for the respective PAPR reduction methods. The number of real multiplications is a function of N, M, F, and L.

Based on Table 1, Fig. 16 shows the average throughput as a function of the number of real multiplications of PCCNC and PAPC for a given PAPR requirement with L as a parameter. The required average PAPR is set to 7 dB. The relationship between the number of real multiplications and the average throughput is varied by changing J for the respective PAPR reduction methods. PCCNC with $L = 32$ reduces the computational complexity required for achieving the same PAPR compared to PCCNC with $L = 1$. This is mainly because the number of power measurement processes that is conducted at each iteration is reduced as L is increased since the number of iterations is decreased thanks to the parallel peak reductions. PCCNC with $L = 64$ increases the computational complexity levels compared to that for $L = 32$. This may be because an excessively high-parallel processing results in inefficient peak reduction due to the peak regrowth caused by the superposition of multiple PC signals. We confirm based on Figs. 15 and 16 that the use of appropriate L parallel processing in PCCNC contributes to not only a reduction in the number of iterations but also a reduction in the computational complexity.

Figure 17 shows the average throughput as a function of the number of real multiplications of the respective PAPR reduction methods for the required average PAPR of 7 dB. L is set to 32 for PCCNC and PAPC. When we focus on PCCNC and CFCNC, PCCNC achieves a better tradeoff between the throughput and computational complexity than CFCNC. The reduction in computational complexity using PCCNC compared to that for CFCNC is enhanced as N is increased. For example, when the target throughput is 32 b/s/Hz at the PAPR of 7 dB with $N = 128$, PCCNC with $L = 32$ reduces simultaneously the number of iterations and computational complexity by approximately 1/3 and 1/25, respectively, compared to those for CFCNC based on Figs. 15 and 17. Therefore, the proposed PCCNC with parallel processing reduces the computational complexity and the number of iterations (in other words, the processing delay time) simultaneously compared to conventional CFCNC or PCCNC without parallel processing while achieving the same PAPR reduction performance.

5. Conclusion

This paper proposed a computational complexity-reduced algorithm called PCCNC with parallel processing for the adaptive PAPR reduction method that uses the null space in a MIMO channel for MIMO-OFDM signals. In the proposed PCCNC, multiple PC signal vectors, which are designed so that they are only transmitted to the null space in the MIMO channel and satisfy the out-of-band radiation requirement, are added to the transmission signal vector to suppress multiple peaks simultaneously at each iteration. When the difference between two target timings of peak signals is excessively small, the peak regrowth caused by the effect of the superposition of the main lobe of multiple PC signals occurs with high probability. To address this issue, the proposed PCCNC with parallel processing restricts the minimum difference between multiple target timings of peak signals. Computer simulation results showed that the proposed PCCNC with the appropriate number of parallel processes along with the restriction on the minimum difference between multiple target timings of peak signals dramatically reduces the required number of iterations compared to the previous algorithm while it achieves comparable PAPR reduction performance with much lower computational complexity. This paper assumes a frequency-nonselective channel as the initial step of the study. Extension of the proposed PCCNC to accommodate a frequency-selective channel is left for future study. When the channel is frequency-selective, the null space of the MIMO channel is also frequency-dependent. Therefore, the BF vector applied to the PC signal at each frequency should be changed so that the PC signal is transmitted only to the null space in the MIMO channel at that frequency. We note that our preliminary work on the extension of the PCCNC to accommodate the frequency-selective fading channel was presented in [30]; however, the parallel processing proposed herein was not considered.

Acknowledgments

A part of this work was supported by the MIC/SCOPE #205003004.

References

[1] T.L. Marzetta, "Noncooperative cellular wireless with unlimited numbers of base station antennas," IEEE Trans. Wireless Commun., vol.9, no.11, pp.3590–3600, Nov. 2010.
[2] H. Papadopoulos, C. Wang, O. Bursalioglu, X. Hou, and Y. Kishiyama, "Massive MIMO technologies and challenges towards 5G," IEICE Trans. Commun., vol.E99-B, no.3, pp.602–621, March 2016.
[3] S.H. Han and J.H. Lee, "An overview of peak-to-average power ratio reduction techniques for multicarrier transmission," IEEE Wireless Commun., vol.12, no.2, pp.56–65, April 2005.
[4] X. Li and L.J. Cimini, Jr., "Effect of clipping and filtering on the performance of OFDM," IEEE Commun. Lett., vol.2, no.5, pp.131–133, May 1998.
[5] A. Gatherer and M. Polley, "Controlling clipping probability in DMT transmission," Proc. 31st Asilomar Conference on Signals, Systems, and Computers, pp.578–584, Nov. 1997.
[6] J. Armstrong, "Peak-to-average power reduction for OFDM by repeated clipping and frequency domain filtering," Electron. Lett., vol.38, no.8, pp.246–247, Feb. 2002.
[7] R.W. Bauml, R.F.H. Fischer, and J.B. Huber, "Reducing the peak-to-average power ratio of multicarrier modulation by selected mapping," Electron. Lett., vol.32, no.22, pp.2056–2057, Oct. 1996.
[8] S.H. Muller and J.B. Huber, "OFDM with reduced peak-to-average power ratio by optimum combination of partial transmit sequences," Electron. Lett., vol.33, no.5, pp.368–369, Feb. 1997.
[9] N. Taşpınar and M. Yıldırım, "A novel parallel artificial bee colony algorithm and its PAPR reduction performance using SLM scheme in OFDM and MIMO-OFDM systems," IEEE Commun. Lett., vol.19, no.10, pp.1830–1833, Oct. 2015.
[10] T. Mata, P. Boonsrimuang, and P. Boontra, "A PAPR reduction scheme based on improved PTS with ABC algorithm for OFDM signal," Proc. 2018 15th International Conference on Electrical Engineering/Electronics, Computer, Telecommunications and Information Technology (ECTI-CON), Chiang Rai, Thailand, July 2018.
[11] J. Tellado and J.M. Cioffi, "Efficient algorithms for reducing PAR in multicarrier systems," Proc. IEEE Int. Symp. Inf. Theory, p.191, Cambridge, MA, Aug. 1998.
[12] H. Lee, D.N. Liu, W. Zhu, and M.P. Fitz, "Peak power reduction using a unitary rotation in multiple transmit antennas," Proc. IEEE ICC2005, pp.2407–2411, Seoul, Korea, May 2005.
[13] G.R. Woo and D. L Jones, "Peak power reduction in MIMO OFDM via active channel extension," Proc. IEEE ICC2005, pp.2636–2639, Seoul, Korea, May 2005.
[14] S. Suyama, H. Adachi, H. Suzuki, and K. Fukawa, "PAPR reduction methods for eigenmode MIMO-OFDM transmission," Proc. IEEE VTC2009-Spring, Barcelona, Spain, April 2009.
[15] C. Studer and E.G. Larsson, "PAR-aware large-scale multi-user MIMO-OFDM downlink," IEEE J. Sel. Areas Commun., vol.31, no.2, pp.303–313, Feb. 2013.
[16] C. Ni, Y. Ma, and T. Jiang, "A novel adaptive tone reservation scheme for PAPR reduction in large-scale multi-user MIMO-OFDM systems," IEEE Wireless Commun. Lett., vol.5, no.5, pp.480–483, Oct. 2016.
[17] H. Prabhu, O. Edfors, J. Rodrigues, L. Liu, and F. Rusek, "A low-complex peak-to-average power reduction scheme for OFDM based massive MIMO systems," Proc. ISCCSP2014, Athens, Greece, May 2014.
[18] Y. Sato, M. Iwasaki, S. Inoue, and K. Higuchi, "Clipping and filtering-based adaptive PAPR reduction method for precoded OFDM-MIMO signals," IEICE Trans. Commun., vol.E96-B, no.9, pp.2270–2280, Sept. 2013.
[19] S. Inoue, T. Kawamura, and K. Higuchi, "Throughput/ACLR performance of CF-based adaptive PAPR reduction method for eigenmode MIMO-OFDM signals with AMC," IEICE Trans. Commun., vol.E96-B, no.9, pp.2293–2300, Sept. 2013.
[20] R. Kimura, Y. Tajika, and K. Higuchi, "CF-based adaptive PAPR reduction method for block diagonalization-based multiuser MIMO-OFDM signals," Proc. IEEE VTC2011-Spring, Budapest, Hungary, May 2011.
[21] Y. Matsumoto, K. Tateishi, and K. Higuchi, "Performance evaluations on adaptive PAPR reduction method using null space in MIMO channel for eigenmode massive MIMO-OFDM signals," Proc. APCC2017, Perth, Australia, Dec. 2017.
[22] M. Suzuki, Y. Kishiyama, and K. Higuchi, "Combination of beamforming with per-antenna power constraint and adaptive PAPR reduction method using null space in MIMO channel for multiuser massive MIMO-OFDM transmission," Proc. WPMC2018, Chiang Rai, Thailand, Nov. 2018.
[23] A. Ivanov, A. Volokhatyi, D. Lakontsev, and D. Yarotsky, "Unused beam reservation for PAPR reduction in massive MIMO system,"

Proc. IEEE VTC2018-Spring, Porto, Portugal, June 2018.
[24] T. Suzuki, M. Suzuki, Y. Kishiyama, and K. Higuchi, "Complexity-reduced adaptive PAPR reduction method using null space in MIMO channel for MIMO-OFDM signals," IEICE Trans. Commun., vol.E103-B, no.9, pp.1019–1029, Sept. 2020.
[25] T. Hino and O. Muta, "Adaptive peak power cancellation scheme under requirements of ACLR and EVM for MIMO-OFDM systems," Proc. IEEE PIMRC2012, Sydney, Australia, Sept. 2012.
[26] T. Kageyama, O. Muta, and H. Gacanin, "An adaptive peak cancellation method for linear-precoded MIMO-OFDM signals," Proc. IEEE PIMRC2015, Hong Kong, Aug.–Sept. 2015.
[27] T. Suzuki, M. Suzuki, Y. Kishiyama, and K. Higuchi, "Parallelly processed peak cancellation signal-based PAPR reduction method using null space in MIMO channel for MIMO-OFDM signals," Proc. IEEE VTC2020-Spring, Antwerp, Belgium, May 2020.
[28] M. Sharif, M. Gharavi-Alkhansari, and B.H. Khalaj, "On the peak-to-average power of OFDM signals based on oversampling," IEEE Trans. Commun., vol.51, no.1, pp.72–78, Jan. 2003.
[29] H. Ochiai and H. Imai, "Performance analysis of deliberately clipped OFDM signals," IEEE Trans. Commun., vol.50, no.1, pp.89–101, Jan. 2002.
[30] L. Yamaguchi, N. Nonaka, and K. Higuchi, "PC-signal-based PAPR reduction using null space in MIMO channel for MIMO-OFDM signals in frequency-selective fading channel," Proc. IEEE VTC2020-Fall, Virtual conference, Nov.–Dec. 2020.

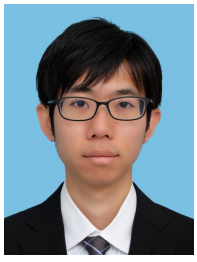

Taku Suzuki received the B.E. and M.E. degrees from Tokyo University of Science, Noda, Japan in 2019 and 2021, respectively. In 2021, he joined Hitachi, Ltd. He is a member of the IEICE.

Mikihito Suzuki received the B.E. and M.E. degrees from Tokyo University of Science, Noda, Japan in 2018 and 2020, respectively. In 2020, he joined NTT DOCOMO, INC. He is a member of the IEICE.

Kenichi Higuchi received the B.E. degree from Waseda University, Tokyo, Japan, in 1994, and received the Dr.Eng. degree from Tohoku University, Sendai, Japan in 2002. In 1994, he joined NTT Mobile Communications Network, Inc. (now, NTT DOCOMO, INC.). While with NTT DOCOMO, INC., he was engaged in the research and standardization of wireless access technologies for wideband DS-CDMA mobile radio, HSPA, LTE, and broadband wireless packet access technologies for systems beyond IMT-2000. In 2007, he joined the faculty of the Tokyo University of Science and currently holds the position of Professor. His current research interests are in the areas of wireless technologies and mobile communication systems, including advanced multiple access, radio resource allocation, inter-cell interference coordination, multiple-antenna transmission techniques, signal processing such as interference cancellation and turbo equalization, and issues related to heterogeneous networks using small cells. He was a co-recipient of the Best Paper Award of the International Symposium on Wireless Personal Multimedia Communications in 2004 and 2007, a recipient of the Young Researcher's Award from the IEICE in 2003, the 5th YRP Award in 2007, the Prime Minister Invention Prize in 2010, and the Invention Prize of Commissioner of the Japan Patent Office in 2015. He is a member of the IEEE.